

# Exclusion of canonical WIMPs by the joint analysis of Milky Way dwarfs with Fermi

Alex Geringer-Sameth\* and Savvas M. Koushiappas†

*Department of Physics, Brown University, 182 Hope St., Providence, RI 02912*

(Dated: April 19, 2022)

Dwarf spheroidal galaxies are known to be excellent targets for the detection of annihilating dark matter. We present new limits on the annihilation cross section of Weakly Interacting Massive Particles (WIMPs) based on the joint analysis of eight Milky Way dwarfs using a frequentist Neyman construction and Pass 7 data from the Fermi  $\gamma$ -ray Space Telescope. We exclude generic WIMP candidates with mass less than 27 GeV that reproduce the observed relic abundance. To within 98% systematic uncertainties this lower limit can be as large as 80 GeV.

PACS numbers: 95.35.+d, 11.30.Rd, 98.80.-k, 95.55.Ka, 07.85.-m

Weakly Interacting Massive Particles (WIMPs) have long been considered well-motivated, and generic candidates for dark matter [1–6]. By virtue of their weak interactions with standard model particles, WIMPs in thermal equilibrium in the early universe “freeze out” by the same mechanism which explains the observed abundance of atomic nuclei. The present-day abundance of WIMPs is governed by their annihilation cross section into standard model particles.

Due to the form of their weak-scale cross section, WIMPs have an abundance of  $\Omega_\chi h^2 \simeq 3 \times 10^{-27} \text{ cm}^3 \text{ s}^{-1} / \langle \sigma_A v \rangle$ , almost irrespective of the mass of the particle [7]. For the measured dark matter density  $\Omega_\chi h^2 \simeq 0.1$  [8], the velocity averaged annihilation cross section must be  $\langle \sigma_A v \rangle \sim 3 \times 10^{-26} \text{ cm}^3 \text{ s}^{-1}$ . Because a smaller cross section overproduces the observed density, this value should be seen as a relatively strong lower bound on  $\sigma_A$  in the canonical thermal WIMP scenario. If observations can lower the upper limit on the cross section below this level, they will present a serious challenge to the conventional WIMP dark matter hypothesis (see e.g., [9–11]).

By now it is well known that Milky Way dwarf galaxies are excellent targets to search for dark matter annihilation signatures. This is because they are dark matter dominated objects with no astrophysical background (few stars and no hot gas). Measurements of the velocity dispersion of stars in these systems allows the reconstruction of the potential well and thus the density profile of the dark matter distribution [12–14].

In order to place constraints on the annihilation cross section, we need to quantify how the value of  $\langle \sigma_A v \rangle$  influences the number of  $\gamma$ -ray events detected with the Large Area Telescope (LAT) onboard the Fermi  $\gamma$ -ray Space Telescope (Fermi). There are two sources of detected photon events: those arising from dark matter annihilation (signal), and those produced by any other processes (background).

In the canonical picture, dark matter annihilates and gives rise to a  $\gamma$ -ray flux which factors into the product of two independent terms: one describing the dark matter particle physics and one involving the astrophysical

properties of the dwarf galaxy. The expected number of detected events from dark matter annihilation in a dwarf galaxy is thus given by

$$\mu(\Phi_{\text{PP}}) = (A_{\text{eff}} T_{\text{obs}}) \times \Phi_{\text{PP}} \times J, \quad (1)$$

where  $A_{\text{eff}}$  is the effective area of the detector and  $T_{\text{obs}}$  is the observation time. The product of these two quantities is called the exposure. The goal is to place limits on the quantity  $\Phi_{\text{PP}}$  which encompasses the particle physics. It is defined as

$$\Phi_{\text{PP}} \equiv \frac{\langle \sigma_A v \rangle}{8\pi M_\chi^2} \int_{E_{\text{th}}}^{M_\chi} \sum_f B_f \frac{dN_f}{dE} dE,$$

where  $M_\chi$  is the mass of the dark matter particle and  $\langle \sigma_A v \rangle$  is its *total* velocity-averaged cross section for annihilation into standard model particles. The index  $f$  labels the possible annihilation channels, and  $B_f$  is the branching ratio for each one. For each channel,  $dN_f/dE$  describes the final  $\gamma$ -ray spectrum, i.e. the number of photons emitted at each energy by the end of the annihilation chain. This quantity is integrated from some threshold energy  $E_{\text{th}}$  to the mass of the dark matter particle.

The quantity  $J$  contains information about the distribution of dark matter, and is defined by

$$J \equiv \int_{\Delta\Omega(\psi)} \int_{\ell} [\rho(\ell, \psi)]^2 d\ell d\Omega(\psi).$$

Here, the square of the dark matter density  $\rho(\ell, \psi)$  is integrated along a line of sight in a direction labeled by  $\psi$ , and over a solid angle  $\Delta\Omega$ .

Typically, the background in the direction of an expected  $\gamma$ -ray source is derived through detailed modeling of the possible contributions that could give rise to a diffuse background [15]. This was the approach taken in the analysis of dwarf galaxies by the Fermi collaboration [16]. In this work we follow a different path. We eschew such detailed modeling of the origin and spectral properties of the  $\gamma$ -ray background, and instead use the photon events

in the region near each dwarf galaxy to empirically derive the distribution describing background events from all unresolved sources.

The fundamental assumption of our strategy is this: *whatever the processes are which give rise to the photon events nearby each dwarf, these same processes are also at work in the direction of the dwarf.* That is, the probability that background processes produce photons at the location of a dwarf can be determined by the empirical probability distribution found by sampling the observed counts in the surrounding region. (In the language of experimental particle physics, the region surrounding each dwarf is a “sideband” used to determine the background.) This approach to the handling of the background requires zero free parameters and the entire analysis depends only on the value of  $\Phi_{\text{PP}}$  which describes the dark matter particle properties.

We use the following eight dwarf galaxies: Bootes I, Draco, Fornax, Sculptor, Sextans, Ursa Major II, Ursa Minor, and Segue 1. This is the same collection of dwarf galaxies that was analyzed by the Fermi collaboration [16], with the addition of Segue 1 and the exception of Coma Berenices (due to its crowded field). For the first 7 dwarfs, we utilize the values of  $J$  quoted in [16] (see Tables 1 and 4 in [16]). For Segue 1 we use the value shown in the preliminary results of the joint analysis of dwarfs by the Fermi collaboration presented in [17]. For all the dwarfs, the  $J$  values are derived based on the modeling of the velocity dispersion profiles of stars in each dwarf [12–14].

We define a Region of Interest (ROI) to be a region of the sky with a radius of  $0.5^\circ$ , which contains all **Pass 7** photon events of **event class 2** available publicly on the Fermi Science Support Center (FSSC) [18] in the Mission Elapsed Time interval of [239557417-334619159] seconds (August 4, 2008 15:43:36 UTC to August 9, 2011 21:45:57 UTC), and with energies in the interval [1-100] GeV (at these energies, the point spread function (PSF) is always less than 1 degree). For a given ROI, we use the publicly available version **v9r23p1** of the **Fermi Science Tools** to extract photons (with **zmax=100**), select good time intervals (with all standard recommendations as stated on the FSSC), generate a light curve, and compute the exposure ( $A_{\text{eff}}T_{\text{obs}}$ ), which also takes into account the shape of the PSF within the ROI using the Instrument Response Function **P7SOURCE\_V6**.

We identify and mask all sources present within  $10^\circ$  of each dwarf using the 2nd Fermi Source Catalogue [19]. We then measure the number of photon events within a ROI centered on each dwarf. We calculate the probability of observing background events at the location of the dwarf by sampling ROI’s which are randomly selected within a distance of  $10^\circ$  from each dwarf, and counting the number of events in each. If a window overlaps with a masked location or with the boundary of the selected data it is rejected. There are approximately  $(10/0.5)^2 =$

400 independent ROIs for each dwarf. The background probability mass function (PMF) is then given by the fraction of ROIs that contained a given number of counts.

The accuracy of this strategy requires that the total exposure does not vary within a  $10^\circ$  radius around each dwarf. We measure the exposure among a collection of ROI’s within each field and find that it varies by at most  $\sim 5\%$ . If a  $\gamma$ -ray source is particularly close to a dwarf it may contribute photons to the central ROI of radius  $0.5^\circ$ . These source photons are not accounted for in the empirical background PMF. Therefore, such photons are considered more likely to be from dark matter annihilation and will weaken the derived upper limit on  $\langle\sigma_{\text{AV}}\rangle$ . In this sense, our analysis is conservative.

In statistical inference, one wants to generate confidence intervals for a model parameter  $\mu$  based on the observed data  $x$ . For a frequentist analysis, the main task is to decide on an *algorithm* which constructs a region in  $\mu$ -space for any value of  $x$ . This region is said to be an  $\alpha$ -confidence interval if the algorithm has “coverage”  $\alpha$  (for an introduction see e.g. [20, 21]).

One way to construct and visualize confidence regions is by using the Neyman construction [21, 22]. The ingredients needed are the parameter space of possible  $\mu$  values, a space of possible measurements  $x$ , and a likelihood function  $P(x|\mu)$ , which gives the probability of observing  $x$  if  $\mu$  were the true value of the parameter ( $\mu$  and  $x$  can both live in any number of dimensions). For each possible value of the parameter  $\mu$  one selects a region  $D(\mu)$  of the measurement space such that  $\int_{D(\mu)} P(x|\mu) = \alpha$  (i.e. the probability of measuring  $x$  to be in  $D(\mu)$  is  $\alpha$  if the true value of the parameter were  $\mu$ ). These regions are called “confidence belts”. For an actual measurement  $x^*$ , these pre-selected belts can be used to generate an  $\alpha$ -confidence region for  $\mu$ . This region is simply the collection of all the  $\mu$  values whose belt  $D(\mu)$  contains  $x^*$ . One sees that this algorithm for constructing a region in  $\mu$ -space out of a measured value  $x^*$  provides the proper coverage: whatever the true value  $\mu_t$  is, there is an  $\alpha$  chance that  $x^*$  will lie in  $D(\mu_t)$  (by construction) and therefore an  $\alpha$  chance that the resulting confidence region will contain  $\mu_t$ .

In this analysis, the observations consist of the number of counts  $N_i$  from the region within a radius of  $0.5^\circ$  of each dwarf ( $i = 1, \dots, 8$ ). These can be considered the components of a vector  $\mathbf{N}$  living in a 8-dimensional integer lattice. To apply the Neyman construction we must choose a confidence belt in this 8-dimensional “ $N$ -space” for every possible value of  $\Phi_{\text{PP}}$ , such that the probability that  $\mathbf{N}$  is measured to be in this belt is  $\alpha$ .

There is complete freedom in the choice of belts (provided they have coverage  $\alpha$ ). However, it is vital that the shape of the belts for each  $\Phi_{\text{PP}}$  not be based on the measured data. This offense was pointed out in [21] and is known as “flip-flopping”. It may result in confidence

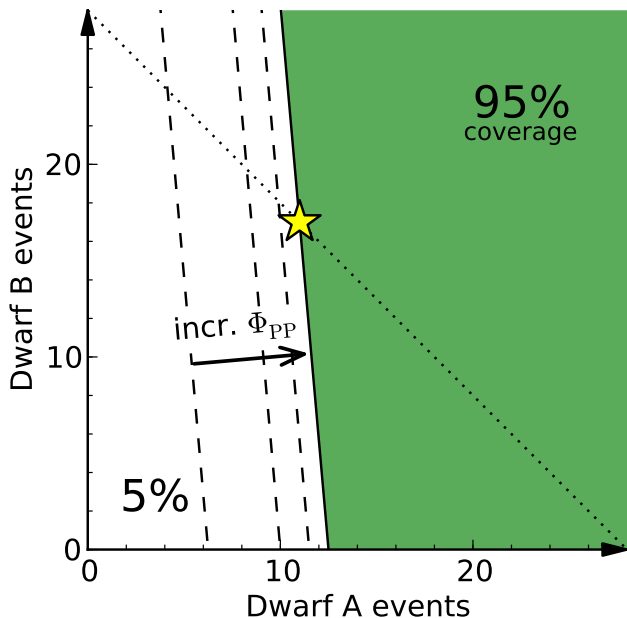


FIG. 1: Illustration of the Neyman confidence belt construction used to generate upper limits on the particle physics parameter  $\Phi_{PP}$ . The “measurement space” is shown, where each axis represents the number of events that could be observed from a given dwarf galaxy (here, Dwarf A has a larger  $J$  value than Dwarf B does). The shaded area, bordered by the solid line, represents the 95%-confidence belt for a particular value of  $\Phi_{PP}$ . The dashed lines are the borders of the confidence belts for different values of  $\Phi_{PP}$ , with  $\Phi_{PP}$  increasing from left to right. The borders are chosen to be normal to a vector of “sensitivities”, which weights each dwarf according to the relative strength of its dark matter signal. Once a measurement is made (shown by the star) the 95% confidence interval for  $\Phi_{PP}$  contains all values of  $\Phi_{PP}$  whose 95%-confidence belt contains the measured point (here, the values of  $\Phi_{PP}$  less than that corresponding to the solid line). The dotted line shows the border for an alternative construction of the confidence belts which gives equal weight to each dwarf.

levels having lower coverage than stated.

In order to derive an upper limit on  $\Phi_{PP}$ , the  $N$ -space should be divided into two simple parts and the belt  $D(\Phi_{PP})$  should consist of the “large”  $\mathbf{N}$  values (i.e. the region containing  $N_i = \infty$ ). This is illustrated in Fig. 1 for an example joint analysis of two dwarfs. The simplest choice for the confidence belt boundaries are planes with normal vectors parallel to  $(1, \dots, 1)$ , represented in Fig. 1 by the dotted line. A measured set of  $N_i$  is in such a confidence belt if the sum of the  $N_i$  is greater than some value. This is equivalent to “stacking” the events from each dwarf on top of one another and then analyzing this single image. However, because the dwarfs are treated equally, photons from a dwarf with a small  $J$  value are considered as likely to have come from dark matter as are photons from a dwarf with large  $J$ . This is clearly an inefficient choice for the confidence belts. Naively, one

extra photon from Draco ( $J \propto 1.20$ ) should raise the upper limit much more than an extra photon from Bootes I ( $J \propto 0.16$ ) because, a priori, a given photon from Bootes I is much more likely to be from background than a photon from Draco.

To overcome this obstacle we take advantage of the recent idea by Sutton [23] to use planes at angles other than  $45^\circ$  as boundaries of the confidence belts. Specifically, Sutton suggests letting the normal vector to the planes be equal to a vector representing the “sensitivity” of each observation. We take the sensitivity (or weight) of each dwarf observation to be proportional to the ratio of the expected dark matter flux ( $A_{\text{eff}} T_{\text{obs}} J$ ) to the mean expected empirical background flux. We note that using weights proportional to  $J$  or to the “signal to noise ratio” of  $J$  to background counts changes the final upper limits on  $\langle \sigma_A v \rangle$  by less than 5%. In contrast, giving every dwarf the same weight weakens the derived upper limits on  $\langle \sigma_A v \rangle$  by about 60%.

The number of photons received in the central  $0.5^\circ$  surrounding each dwarf is the sum of the number of photons produced via dark matter annihilation and the number of photons produced by all background processes. The number of signal photons is governed by a Poisson distribution with mean given by  $\mu(\Phi_{PP})$  (Eq. 1). The number of background photons received is described by the empirical distribution derived from the region surrounding each dwarf. Therefore, the total number of photons detected is distributed according to the convolution of these two probability distributions. Finally, the counts found for each dwarf galaxy are independent variables and so the joint probability of measuring  $\mathbf{N}$  is given by the product of the individual PMFs for each dwarf.

Using the aforementioned statistical framework we derive an upper bound of  $\Phi_{PP} = 7.3^{+2.5}_{-5.2} \times 10^{-30} \text{ cm}^3 \text{ s}^{-1} \text{ GeV}^{-2}$  at 95% confidence. In order to translate the bound on  $\Phi_{PP}$  into a bound on  $\langle \sigma_A v \rangle$  as a function of the WIMP mass we need to assume a specific annihilation channel and its spectrum  $dN/dE$ . For example, a supersymmetric WIMP may have annihilation branching ratios into hadrons (e.g.  $b\bar{b}$ ) or into leptons (e.g.  $\tau\bar{\tau}$ ), which then decay by fairly well-constrained channels into  $\gamma$ -rays. We adopt the  $dN/dE$  fitting forms given in [24].

Figure. 2 shows the derived 95% upper bound on  $\langle \sigma_A v \rangle$  as a function of WIMP mass. The dominant source of systematic uncertainty comes from the poorly constrained  $J$  values for each dwarf and is shown by the shaded regions in Fig. 2. The  $\Phi_{PP}$  limit is recalculated for each dwarf as its  $J$  value varies between its upper and lower 98% error bar given in [16, 17]. The results for each dwarf are then added in quadrature to get the total systematic uncertainty quoted above. (This procedure gives a nearly identical region as that derived by scanning over the log-normal priors on  $J$  for each dwarf as is done in [17].) Segue 1 is responsible for most of the uncertainty

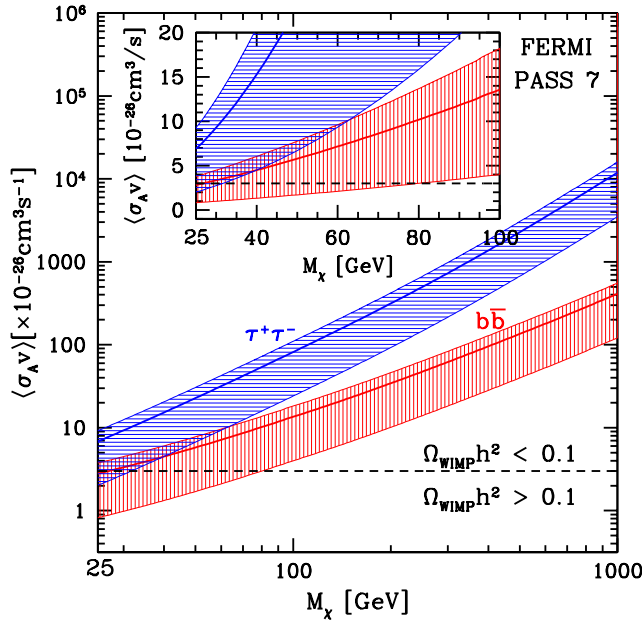


FIG. 2: Derived 95% upper limit on  $\langle\sigma_A v\rangle$  as a function of mass for dark matter annihilation into  $b\bar{b}$  and  $\tau^+\tau^-$ . The shaded area reflects the 98-percentile of the systematic uncertainty in the dark matter distribution of the dwarfs. The canonical annihilation cross section for a thermal WIMP making up the total observed dark matter abundance is shown by the dashed line. The inset figure shows detail for lower masses.

in the limit and the lopsided shaded region is caused by the asymmetric (log-normal) distribution assumed for its  $J$  value.

Including the uncertainties in  $J$  in this way can be regarded as a sort of hybrid frequentist-Bayesian effort. If we knew the exact  $J$  value of each dwarf, the width of the shaded regions in Fig. 2 would shrink to zero and we would have a purely frequentist upper limit on  $\langle\sigma_A v\rangle$  (i.e., there will be only a 5% change that the cross section is higher than the stated limit). However, due to the uncertainties in  $J$ , we have no knowledge of where this upper limit lies within the shaded region. Presenting the limit in this fashion clearly separates the inherent statistical uncertainties (Poisson-distributed photon counts) from the systematic errors in the  $J$ 's, which in principle could be known exactly (each dwarf has “a” dark matter distribution).

It is important to emphasize that Draco and Ursa Minor are the dominant dwarfs determining the derived central value upper limit (solid lines in Fig. 2). This is due to the fortuitous combination of large  $J$  values and low background contributions from these dwarfs. In fact, if the analysis were carried out with Draco and Ursa Minor *only* the “95%” upper limit would get stronger by about 60%. However, as pointed out in [21] we may not pick and choose which dwarfs to include after the fact without altering the confidence level of the bound. The weight-

ing scheme we have employed allows us to quote true 95% confidence limits while making a minimal sacrifice to the strength of the upper limit on  $\langle\sigma_A v\rangle$ .

The strength of the analysis relies on the validity of the assumption that the background PMF at the location of each dwarf is adequately described by the empirical PMF derived from the region near the dwarf. In general, if the assumed background PMF is skewed toward higher numbers of counts the upper limit on  $\Phi_{\text{PP}}$  becomes stronger. This is because more of the observed counts can be attributed to background and therefore fewer to dark matter annihilation. We can quantify the effect of an error in the empirical PMF by considering the radical case where there is no background at all. Clearly this is a false assumption, but is one which will produce the most conservative (i.e. weakest) limit on  $\Phi_{\text{PP}}$ . If we force the background PMFs to be equal to 1 when the number of counts is 0 and 0 otherwise, the 95% limit on  $\Phi_{\text{PP}}$  increases by a factor of about 6.6 over the actual limit. This represents the case where every photon received from a dwarf is believed to be the product of dark matter annihilation. While this would, of course, push the derived upper limit on  $\langle\sigma_A v\rangle$  above the canonical value of  $3 \times 10^{-26} \text{cm}^3 \text{s}^{-1}$ , we interpret this as a test of the robustness of the method, not as any sort of actual confidence limit.

We can also test our conclusions against less violent changes to the background PMF. For each dwarf we replaced the background PMF with a Poisson distribution having the same mean, and found that the limit on  $\Phi_{\text{PP}}$  decreases by about 18%. These tests of the empirical PMF, perhaps overly simplistic, do give us the sense that the derived limit is robust and can be justified as an additional piece of evidence in the dark matter search endeavor.

What is the significance of this new bound on  $\langle\sigma_A v\rangle$ ? It signals, perhaps, that we are imminently approaching an epoch of discovery. Three decades of experimental design have given rise to many detectors sensitive enough to probe a very generic class of dark matter candidates. The prime motivation for WIMP dark matter is the coincidence that a weak-scale annihilation cross section naturally reproduces the observed relic abundance. Unlike the scattering cross section probed in direct detection experiments, cosmology gives a lower limit for the annihilation cross section based on the requirement that WIMPs are not more abundant than observed. The parameter space in which a WIMP can hide is therefore bounded at both ends. This work pushes the contact point between the upper and lower bounds on  $\langle\sigma_A v\rangle$  to increasing WIMP masses, suggesting that we have reached the stage where our observations have become powerful enough to either discover or rule out the best-motivated and most sought-after dark matter candidate.

We acknowledge useful conversations with John Beacom, Elizabeth Hays, Andrew Hearin, Julie McEnery,

Tim Tait and Andrew Zentner. AGS and SMK are supported by NSF grant PHY-0969853 and by Brown University.

---

\* Electronic address: alex.geringer-sameth@brown.edu

† Electronic address: koushiappas@brown.edu

- [1] Y. B. Zel'dovich, Zh. Eksp. Teor. Fiz **48**, 986 (1965).
- [2] Y. B. Zel'dovich et al., Usp. Fiz. Nauk. **84**, 113 (1965).
- [3] B. W. Lee and S. Weinberg, Phys. Rev. Lett. **39**, 165 (1977).
- [4] J. E. Gunn, B. W. Lee, I. Lerche, D. N. Schramm, and G. Steigman, ApJ **223**, 1015 (1978).
- [5] G. Steigman, C. L. Sarazin, H. Quintana, and J. Faulkner, AJ **83**, 1050 (1978).
- [6] J. Ellis, J. S. Hagelin, D. V. Nanopoulos, K. Olive, and M. Srednicki, Nuclear Physics B **238**, 453 (1984).
- [7] G. Jungman, M. Kamionkowski, and K. Griest, Phys. Rep. **267**, 195 (1996).
- [8] E. Komatsu, K. M. Smith, J. Dunkley, C. L. Bennett, B. Gold, G. Hinshaw, N. Jarosik, D. Larson, M. R. Nolte, L. Page, et al., ApJS **192**, 18 (2011).
- [9] M. Cirelli, F. Iocco, and P. Panci, J. Cosmology Astropart. Phys. **10**, 9 (2009).
- [10] K. N. Abazajian, S. Blanchet, and J. P. Harding, ArXiv e-prints (2010).
- [11] K. N. Abazajian, P. Agrawal, Z. Chacko, and C. Kilic, J. Cosmology Astropart. Phys. **11**, 41 (2010).
- [12] L. E. Strigari, S. M. Koushiappas, J. S. Bullock, and M. Kaplinghat, Phys. Rev. D **75**, 083526 (2007).
- [13] L. E. Strigari, S. M. Koushiappas, J. S. Bullock, M. Kaplinghat, J. D. Simon, M. Geha, and B. Willman, ApJ **678**, 614 (2008).
- [14] G. D. Martinez et al., J. Cosmology Astropart. Phys. **6**, 14 (2009).
- [15] A. A. Abdo, M. Ackermann, M. Ajello, E. Antolini, L. Baldini, J. Ballet, G. Barbiellini, D. Bastieri, B. M. Baughman, K. Bechtol, et al., ApJ **720**, 435 (2010).
- [16] A. A. Abdo et al., ApJ **712**, 147 (2010).
- [17] (2011), URL [http://fermi.gsfc.nasa.gov/science/symposium/2011/program/session9/LlenaGarde\\_FermiSymp.pdf](http://fermi.gsfc.nasa.gov/science/symposium/2011/program/session9/LlenaGarde_FermiSymp.pdf).
- [18] (2011), URL <http://fermi.gsfc.nasa.gov/ssc/data/>.
- [19] (2011), URL [http://fermi.gsfc.nasa.gov/ssc/data/access/lat/2yr\\_catalog/2FGL\\_catalog\\_draft\\_v4.2nl.pdf](http://fermi.gsfc.nasa.gov/ssc/data/access/lat/2yr_catalog/2FGL_catalog_draft_v4.2nl.pdf).
- [20] A. Stuart and K. J. Ord, *Kendall's advanced theory of statistics* (Oxford University Press, New York, 1987), 5th ed.
- [21] G. J. Feldman and R. D. Cousins, Phys. Rev. D **57**, 3873 (1998).
- [22] J. Neyman, Royal Society of London Philosophical Transactions Series A **236**, 333 (1937).
- [23] P. J. Sutton, Classical and Quantum Gravity **26**, 245007 (2009).
- [24] J. A. R. Cembranos, A. de La Cruz-Dombriz, A. Dobado, R. A. Lineros, and A. L. Maroto, Phys. Rev. D **83**, 083507 (2011).